Electron-phonon coupling in cuprate high-temperature superconductors determined from exact electron relaxation rates. Supplementary material.

C. Gadermaier[1], A. S. Alexandrov[2,1], V. V. Kabanov[1], P. Kusar[1], T. Mertelj[1], X. Yao[3], C. Manzoni[4], D. Brida[4], G. Cerullo[4], and D. Mihailovic[1]
[1]*Josef Stefan Institute 1001, Ljubljana, Slovenia*
[2]*Department of Physics, Loughborough University, Loughborough LE11 3TU, United Kingdom*
[3]*Department of Physics, Shanghai Jiao Tong University, 800 Dong Chuan Road, Shanghai 200240, China*
[4]*National Laboratory for Ultrafast and Ultraintense Optical Science, INFM-CNR, Dipartimento di Fisica, Politecnico di Milano, 20133 Milano, Italy*

A. Sample preparation

The $YBa_2Cu_3O_{6.5}$ (YBCO) single crystal used here was grown by top-seeded solution growth using a Ba_3Cu_5O solvent[1]. The as-grown single crystal was first annealed at 700 °C for 70 h with flowing oxygen and quenched down to room temperature. The $La_{1.85}Sr_{0.15}CuO_4$ (LSCO) single crystal was synthesised by a travelling-solvent-floating-zone method utilizing infrared radiation furnaces (Crystal system, FZ-T-4000) and annealed in oxygen gas under ambient pressure at 600 °C for 7 days[2].

B. Femtosecond pump-probe set-up

A detailed description of the set-up used is found in[3]. In a "pump-probe" experiment, a "pump" pulse excites the sample and the induced change in transmission or reflection of a delayed probe pulse monitors the relaxation behaviour. In the linear approximation $\frac{\Delta R}{R}$ directly tracks the electronic relaxation processes, and the time constants obtained from fits of its dynamics are the characteristic times of the underlying relaxation processes. In our data, this approximation is justified by two essential characteristics: (i) the $\frac{\Delta R}{R}$ amplitude is linear in the excitation intensity (see Figure 1a for LSCO), and (ii) the same decay times appear independently of the probe wavelength, only with different spectral weights of the individual components.

In order to resolve the dynamics of fast processes very short pulses are necessary, since the instrumental response function is given by the cross correlation between the pump and probe pulses. We use sub-10 fs probe pulses from an ultrabroadband (covering a spectral range from 500 to 700 nm) non-collinear optical parametric amplifier (NOPA) and ∼15 fs pump pulses from a narrower band (wavelength tunable, in our case centred at 530 nm) NOPA. The seed pulses for the NOPAs and the amplified pulses are steered and focussed exclusively with reflecting optics to avoid pulse chirping.

A schematic of the experimental apparatus is shown in Fig. 1. The laser source is a regeneratively amplified modelocked Ti:sapphire laser (Clark-MXR Model CPA-1), delivering pulses at 1 kHz repetition rate with 780 nm center wavelength, 150 fs duration, and 500 μJ energy. Both NOPAs are pumped by the second harmonic of the Ti:sapphire laser, which is generated in a 1-mm-thick lithium triborate crystal (LBO), cut for type-I phase matching in the XY plane ($\theta = 90°$, $\varphi = 31.68°$, Shandong Newphotons).

The ultrabroadband visible NOPA that generates the probe pulses has been described in detail before[4]; a schematic of it is shown in Fig. 2. The white light continuum seed pulses are generated by a small fraction of the fundamental

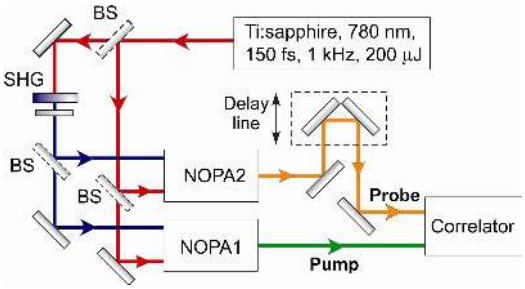

Figure 1: Block scheme of the experimental setup. BS: beam splitter. SHG: second harmonics generation. (redrawn from [3]).

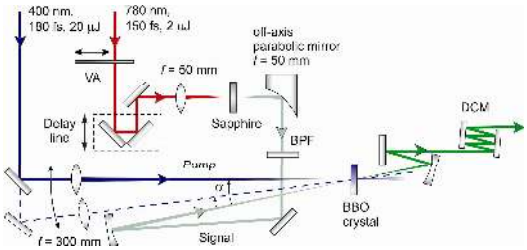

Figure 2: Setup of the noncollinear optical parametric amplifier. BPF: short pass filter that transmits only the visible part of the white light continuum and cuts out the fundamental and infrared components. (redrawn from [3]).

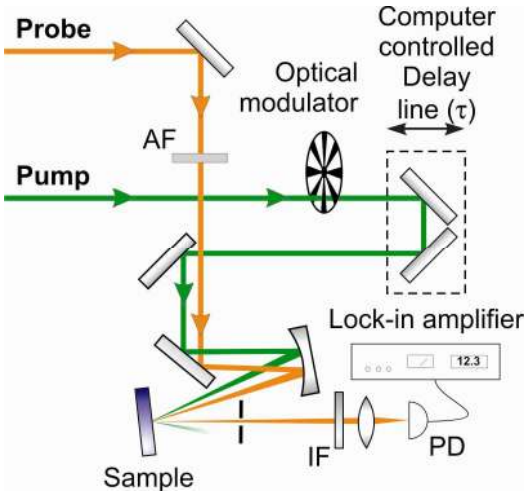

Figure 3: Schematics of the experimental apparatus used for auto/ cross-correlation and pump-probe experiments. AF: attenuating filter. IF: interference filter. PD: photodiode. (redrawn from [3]).

wavelength beam focused into a 1 mm thick sapphire plate. Parametric gain is achieved in a 1-mm-thick BBO crystal, cut at $\theta = 32^{\circ}$, which is the angle giving the broadest phase matching bandwidth for the noncollinear type-I interaction geometry; a single-pass configuration is used to maximize the gain bandwidth. The amplified pulses have energy of approximately 2 μJ and peak-to-peak fluctuations of less than 5%.

The compressor for the ultrabroadband NOPA consists of two custom-designed double-chirped mirrors (DCMs), manufactured by ion-beam sputtering (Nanolayers GmbH), which are composed of 30 pairs of alternating SiO2 /TiO2 quarter-wave layers in which both the Bragg wavelength and the layer duty cycle are varied from layer pair to layer pair. The DCMs introduce a highly controlled negative group delay (GD) over bandwidths approaching 200 THz, compensating for the GD of the NOPA pulses.

The narrower bandwidth NOPA providing the pump pulses is built identically to the one described above, only the amplified bandwidth is reduced by choosing a suitable non-optimum angle between pump and signal beams (dashed path of the blue pump in Figure 2). The pulses are compressed by DCMs similar to those used for the broadband NOPA.

A schematic of the apparatus used for pulse characterization and pump-probe experiments (correlator in Fig. 1) is shown in Fig. 3. The delay line is formed by two 90° turning mirrors mounted on a precision translation stage with 0.1 μm positioning accuracy (Physik Instrumente GmbH, model M-511.DD), which corresponds to 0.66 fs time resolution. The two pulses are combined and focused on the sample by a silver spherical mirror (R=200 mm). The non-collinear configuration enables to spatially separate pump and probe beams. Upon reflection from the sample, the probe beam is selected by an iris and steered to the detector, either a silicon photodiode preceded by a 10 nm spectral width interference filter or an optical multichannel analyzer (OMA). The differential reflection (transmission) signal is obtained via synchronous detection (lock-in amplifier Stanford SR830 for the photodiode, custom made software for the OMA) referenced to the modulation of the pump beam at 500 Hz by a mechanical chopper (Thorlabs MC1000). This allows detection of differential reflection (ΔR/R) signals as low as 10^{-4}.

C. Estimate of the electron-electron relaxation time

The applicability of the FL theory has been somewhat controversal in cuprate superconductors. The recent unambiguous observation of de Haas – van Alphen oscillations[5] has shown that the Fermi surface is almost cylindrical. In this quasi-two-dimensional case the electrons can be described as a FL if $r_s = a/a_B < 37$, with a being the mean electron distance and a_B the Bohr radius[6]. We determine $a = 1/\sqrt{n} = \sqrt{2\pi}/k_F$, with $k_F = 7.4$ nm^{-1} from[5]. Using $a_B = \hbar^2\epsilon_{eff}/m^*e^2$, with $m^* = 4m_e$ and the effective dielectric constant $\epsilon_{eff} \approx 30$, we obtain $r_s \approx 1$, safely in the FL regime.

Compared to a simple FL, e-e correlations increase the effective mass of carriers (or decrease the bare band-width), and heavier carriers form lattice polarons at a smaller value of l. Both spin and lattice polarons have the same Fermi surface as free electrons, but the Fermi energy is reduced [12]. Our (Boltzmann) relaxation theory is based on the existence of the Fermi surface and the Pauli exclusion principle, which the dressed (polaronic) carriers obey like free electrons. Therefore, Equation 3 of the main paper and all our subsequent considerations are valid also for polarons in the presence of strong electron correlations.

In the weak photoexcitation regime where only a small fraction of conduction electrons is excited ($k_BT_e \ll E_F$), e-e scattering is impeded since the Pauli exclusion principle strongly limits the number of available final states. The e-e relaxation time τ_{e-e} can be estimated by: $1/\tau_{e-e} \approx \pi^3\mu_c^2(k_BT_e)^2/4\hbar E_F$ [7], where $\mu_c = r_s/2\pi$ is the Coulomb pseudopotential characterising the electron-electron interaction. Even in the weak photoexcitation regime, the effective T_e after excitation can differ significantly from room temperature. Assuming an electronic specific heat of 1.4 mJ/g.at.K^2 [13], and a pump laser penetration depth of 150 nm, one can estimate $T_e \approx 400$ K, $\tau_{e-e} \approx 1.4$ ps for the lowest and $T_e \approx 800$ K, $\tau_{e-e} \approx 350$ fs for the highest pump fluence used in Fig. 1a of the main manuscript.

D. Exact relaxation rates

Here, differently from previous studies based on the two-temperature model (TTM), we analyze pump-probe relaxation rates using an analytical approach to the Boltzmann equation [8], which is free of any quasi-equilibrium approximation. Due to the complex lattice structure of cuprate superconductors characteristic phonon frequencies spread over a wide interval $\hbar\omega/k_B \gtrsim 200 \div 1000$ K. Very fast oxygen vibrations with frequencies $\omega \gtrsim 0.1/fs$ do not contribute to the relaxation on the relevant time scale, but just dress the carriers. For the remaining part of the spectrum we can apply the Landau-Fokker-Planck expansion, expanding the e-ph collision integral at room or higher temperatures in powers of the relative electron energy change in a collision with a phonon, $\hbar\omega/(\pi k_BT) \lesssim 1$. Then the integral Boltzmann equation for the nonequilibrium part of the electron distribution function $\phi(\xi,t) = f(\xi,t) - f_0(\xi)$ is reduced to a partial differential equation in time-energy space [8]:

$$\gamma^{-1}\dot{\phi}(\xi,t) = \frac{\partial}{\partial\xi}\left[\tanh(\xi/2)\phi(\xi,t) + \frac{\partial}{\partial\xi}\phi(\xi,t)\right], \tag{1}$$

where $f(\xi,t)$ is the non-equilibrium distribution function, and $\gamma = \pi\hbar\lambda\langle\omega^2\rangle/k_BT$. The electron energy, ξ, relative to the equilibrium Fermi energy is measured in units of k_BT. Here $\lambda\langle\omega^2\rangle$ is the second moment of the familiar Eliashberg spectral function [9], $\alpha^2F(\omega)$, defined for any phonon spectrum as:

$$\lambda\langle\omega^n\rangle \equiv 2\int_0^\infty d\omega\frac{\alpha^2F(\omega)\omega^n}{\omega}. \tag{2}$$

The coupling constant λ, which determines the critical temperature of the BCS superconductors, is $\lambda = 2\int_0^\infty d\omega\alpha^2F(\omega)/\omega$.

Multiplying Eq.(1) by ξ and integrating over all energies yield the rate of the energy relaxation:

$$\dot{E}_e(t) = -\gamma\int_{-\infty}^{\infty} d\xi\tanh(\xi/2)\phi(\xi,t), \tag{3}$$

where $E_e(t) = \int_{-\infty}^{\infty} d\xi\xi\phi(\xi,t)$ and $\phi(\xi,t)$is the solution of Eq. 1. Apart from a numerical coefficient the characteristic e-ph relaxation rate (proportional to γ) is about the same as the TTM energy relaxation rate [10], $\gamma_T = 3\hbar\lambda\langle\omega^2\rangle/\pi k_BT$.

To establish the numerical coefficient we solved Eq.(1) and fitted the numerically exact energy relaxation by a near-exponential decay $E(t) = E_0\exp(-at\gamma - bt^2\gamma^2)$, with the coefficients $a = 0.14435$ and $b = 0.00267$, which are virtually independent of the initial distribution, $\phi(\xi,0)$ and pump energy, E_0. The exact relaxation time $\tau = 1/a\gamma$ turns out longer than the TTM relaxation time γ_T^{-1}, by a factor of 2, (see Fig. 4), $\tau = 2\pi k_BT/3\hbar\lambda\langle\omega^2\rangle$. This as well as the shorter relaxation times observed in our ultra-fast pump-probe measurements lead to essentially higher values of EPI coupling constants compared with previous studies.

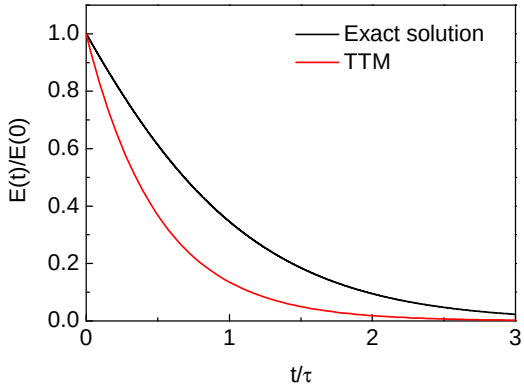

Figure 4: Numerically exact energy relaxation rate compared with TTM rate. E_0 is the pump energy, $\tau = 2\pi k_B T/3\hbar\lambda\langle\omega^2\rangle$ is the exact relaxation time.

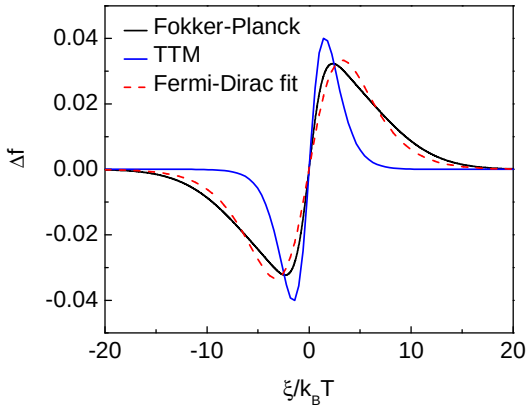

Figure 5: Difference $\Delta f = f(\xi, t = \gamma^{-1}) - f_0(\xi)$ of the transient distribution functions $f(\xi, t = \gamma^{-1})$ and the equilibrium Fermi-Dirac function $f_0(\xi)$. $f(\xi, t)$ is calculated from the Fokker-Planck equation and via the TTM, respectively.

E. Exact transient electron distribution function

In the TTM e-e collision creates a quasi-equilibrium electron distribution that subsequently cools down via e-ph interaction and electron diffusion. On the other hand, in our relaxation scheme, which is dominated by e-ph interaction, the electron distribution during relaxation is not a quasi-equilibrium one. The *deviation* of both functions from the equilibrium is shown in Fig. 5, for $t = \gamma^{-1}$. Since we limit our discussion to the linear regime, the TTM correction to the distribution function is $\Delta f \propto x/cosh(x^2/4)$, where $x = \xi/k_B T$. The width of the two lobes in Δf indicate the effective electronic temperature. The significantly narrower lobes for the TTM compared to the exact distribution illustrate how the TTM underestimates the transient electronic temperature and hence the relaxation time. However, the e-ph dominated relaxation is not just a slower relaxation through the same quasi-equilibrium states as assumed by the TTM. We illustrate this by fitting our non-equilibrium distribution with a quasi-equilibrium one (dashed line in Fig. 5). Since the Fokker-Planck equation describes diffusion in the energy space the high energy tails are clearly seen in our distribution, which, compared to the Fermi-Dirac distribution have a much gentler fall-off towards high electron energies.

While in the deviation from the equilibrium distribution, the difference between the two models is clearly visible, the Fermi-Dirac distribution and the one obtained from solving the Fokker-Planck equation, themselves look rather similar, except for the high energy tail, as can be seen in Fig. 6a. This shines new light on fs ARPES experiments, which directly measure the transient electron distributions. Until now it was customary to use the TTM to describe electron relaxation, ARPES data were in good agreement and were invoked as confirmation of the ultrafast e-e thermalization. We have now shown that a *similar* distribution can be obtained also as a result of e-ph scattering. In Fig. 6b we redraw the best available time-resolved ARPES data for cuprate superconductors [11] together with their fit to a quasi-equilibrium Fermi-Dirac distribution, from which they estimate a hot electron temperature. The spectrum was taken immediately after excitation (at the end of the pump-probe pulse overlap, which is about $\tau/2$

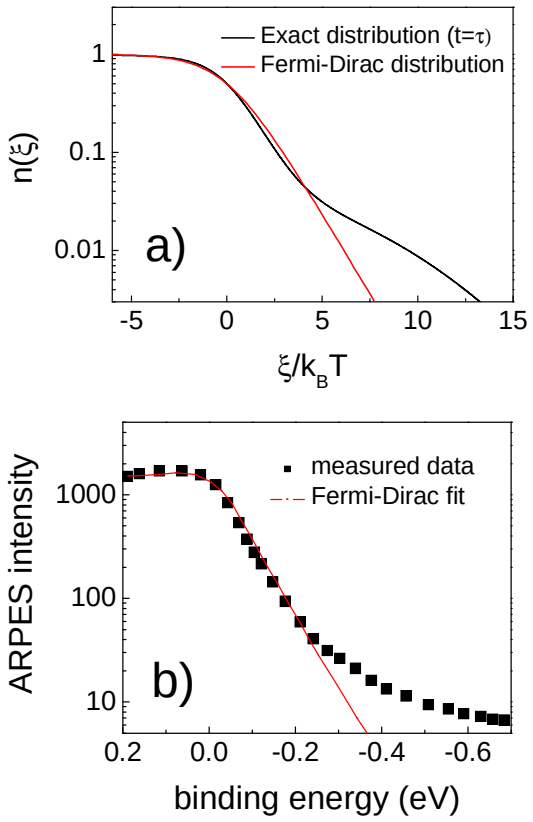

Figure 6: a) Numerically exact distribution function $f(\xi, t = \gamma^{-1})$ compared to a Fermi-Dirac distribution function with the same effective temperature. b) ARPES spectrum of $Bi_2Sr_2CaCu_2O_8$immediately after excitation and fit to a Fermi-Dirac function (redrawn from [11]).

of their decay time after maximum pump-probe overlap, i.e. on average the electrons are probed $\tau/2$ after their excitation). Compared to the Fermi-Dirac curve, their data show a high-energy tail very similar to the exact non-equilibrium distribution we calculated. This means that our relaxation scheme is not only more justified than the TTM on the basis of the physical reasoning described in the main text, it also agrees better with experimental data in the literature. This should in no way derogate the work done before our model was available, however, we propose to reassess quantitative conclusions along the lines of our relaxation scheme (see section G).

F. Predictions of BCS theory

The most common expression that relates EPI to T_c is the BCS-McMillan formula $k_B T_c = \hbar\omega_0 \exp[-(1+\lambda)/\lambda]$ (if any repulsive Coulomb pseudopotential is neglected), where ω_0 is a characteristic phonon frequency. Formally setting $\lambda\langle\omega^2\rangle = \lambda\omega_0^2$, one can rewrite this as a function of $\lambda\langle\omega^2\rangle$ and λ: $k_B T_c = \hbar\sqrt{\lambda\langle\omega^2\rangle/\lambda}\exp[-(1+\lambda)/\lambda]$. Since $\lambda\langle\omega^2\rangle$ is known from experiment, we keep it fixed and find a maximum $T_c(\lambda)$ (by finding a zero of the first derivative) at $\lambda = 2$. T_c as function of λ is shown in Fig 7 for both YBCO and LSCO, the maximum critical temperatures are $T_c^{max} = 52$ K for LSCO and $T_c^{max} = 37$ K forYBCO. For the more realistic estimates given in the main text, $\lambda = 0.5$ for LSCO and $\lambda = 0.25$ for YBCO, we obtain lower T_c values of 23 K and 3 K, respectively. Hence, contrary to experiment BCS theory predicts a lower T_c for YBCO than for LSCO. It cannot explain the high T_c value of YBCO (even for $\lambda = 2$) and the reasonable agreement for LSCO is probably a coincidence.

G. Assessment of lambda values obtained with the TTM and with our model

We now assess the quantitative differences between the values for $\lambda\langle\omega^2\rangle$ (and consequently the estimates for λ that are usually made on their basis) obtained from data analysis using the TTM and our model. The differences between

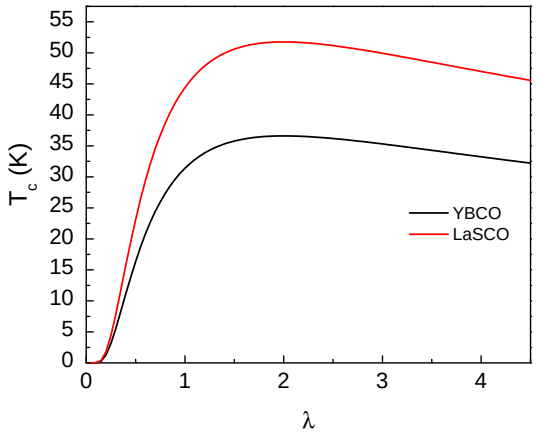

Figure 7: Critical temperature according to the BCS-McMillan formula as a function of λ for $YBa_2Cu_3O_{6.5}$ ($\lambda\langle\omega^2\rangle = 400$ meV^2) and $La_{1.85}Sr_{0.15}CuO_4$ ($\lambda\langle\omega^2\rangle = 800$ meV^2)

Table I: $\lambda\langle\omega^2\rangle$ obtained via the TTM and the Kabanov-Alexandrov (K-A) model from our data on $YBa_2Cu_3O_{6.5}$ and $La_{1.85}Sr_{0.15}CuO_4$ and from [14]. τ_{e-e} are calculated as in section C, τ_{e-ph} from [14] are recalculated from published $\lambda\langle\omega^2\rangle$ and T_e values.

material	T_e (K)	τ_{e-e} (fs)	τ_{e-ph} (fs)	$\lambda\langle\omega^2\rangle_{TTM}$ (meV^2)	$\lambda\langle\omega^2\rangle_{K-A}$ (meV^2)
$YBa_2Cu_3O_{6.5}$	400-800	350-1400	100	400±150	400±100
$La_{1.85}Sr_{0.15}CuO_4$	400-800	350-1400	45	800±300	800±200
Cu	590	3300	1400	29	29
Au	650	1700	1900	23	21
Cr	720		380	130	110
W	1200		710	110	60
V	700		170	280	240
Nb	790	1000	170	320	240
Ti	820		160	350	260
Pb	570	6400	840	45	47
NbN	1070		110	640	360
V3Ga	1110		200	370	200

the analytic expressions that link τ_{e-ph} and $\lambda\langle\omega^2\rangle$ (equations 1 and 2 of the main manuscript) are a factor 2 and that τ_{e-ph} scales with the electron temperature T_e in the TTM and with the lattice temperature T_l in our model. As described in section C, T_l is usually very close to the sample temperature without photoexcitation, while T_e can be several 100 K higher, depending on the excitation conditions. For the fluences we used, $T_e = 600 \pm 200$ K, which introduces an additional uncertainty in $\lambda\langle\omega^2\rangle$ if we use the TTM estimate. The factor 2 in the equations incidentally cancels with the factor 2 in the temperatures.

Brorson et al. studied a series of metallic superconductors, using a quite diverse range of excitation conditions [14]. We list their data together with ours in Table 1. Their T_e values scatter from 570 to 1200 K, hence the differences between the TTM and our model can be up to a factor of 2. Unfortunately they did not study any intensity dependence, so we cannot use this criterion to decide which relaxation scheme is more appropriate. However, we estimate τ_{e-e} as described in section C for four of their samples, using r_s and E_F from [7] and obtain $\tau_{e-e} > \tau_{e-ph}$ in three cases, and $\tau_{e-e} \approx \tau_{e-ph}$ for Au. Therefore, one can assume that except for materials with very low EPI, our model is more appropriate, as has already been established in textbooks like [7].

H. Universality of the observed behavior

In the main paper we show intensity and wavelength dependent pump-probe time traces and show that the dynamics does not change with intensity and that the same characteristic time scales are found at different wavelengths. However, there we show only a few selected wavelengths out of a more comprehensive dataset. To illustrate that the

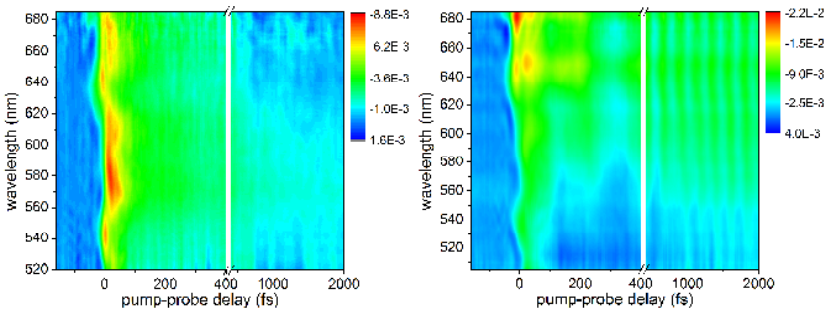

Figure 8: Transient photoinduced reflectivity change $\Delta R/R$ of $La_{1.85}Sr_{0.15}CuO_4$ (a) and $YBa_2Cu_3O_{6.5}$ (b) at a pump intensity of 200 $\mu J/cm^2$.

behavior discussed in the main paper is universal, we show two-dimensional maps of the photoinduced $\Delta R/R$ as a function of probe wavelength and delay for both materials in Figure 8.

[1] X. Yao, T. Mizukoshi, M. Egami, Y. Shiohara, *Physica C* **263**, 197 (1996).
[2] S. Sugai, H. Suzuki, Y. Takayanagi, T. Hosokawa, N. Hayamizu, *Phys. Rev. B* **68** 184504 (2003).
[3] C. Manzoni, D. Polli, G. Cerullo, *Rev. Sci. Instrum.* **77**, 023103 (2006).
[4] G. Cerullo, S. De Silvestri, *Rev. Sci. Instrum.* **74**, 1 (2003).
[5] B. Vignolle *et al.*, *Nature* **455**, 952 (2008).
[6] B. Tanatar and D. M. Ceperley, *Phys. Rev. B* **39**, 5005 (1989).
[7] N. W. Ashcroft and N. D. Mermin *Solid State Physics* (Harcourt, Orlando, 1976).
[8] V. V. Kabanov, A. S. Alexandrov, *Phys. Rev. B* **78** 174514 (2008).
[9] G. M. Eliashberg, *Zh. Eksp. Teor. Fiz.* **38**, 966 (1960); **39**, 1437 (1960) [*Sov. Phys. JETP.* **11**, 696; **12**, 1000 (1960)].
[10] P. B. Allen, *Phys. Rev. Lett.* **59**, 1460 (1987).
[11] L. Perfetti, *et al.*, *Phys. Rev. Lett.* **99**, 197001 (2007).
[12] A. Paramekanti, M. Randeria, and N. Trivedi, *Phys. Rev. Lett.* **87**, 217002 (2001).
[13] J. W. Loram, K. A. Mirza, J. R. Cooper, and W. Y. Liang, *Phys. Rev. Lett.* **71**, 1740 (1993).
[14] Brorson, S.D. et al. *Phys. Rev. Lett.* **64**, 2172 (1990).

Electron-Phonon Coupling in High-Temperature Cuprate Superconductors Determined from Electron Relaxation Rates

C. Gadermaier,[1,*] A. S. Alexandrov,[2,1] V. V. Kabanov,[1] P. Kusar,[1] T. Mertelj,[1] X. Yao,[3] C. Manzoni,[4] D. Brida,[4] G. Cerullo,[4] and D. Mihailovic[1]

[1] *Department of Complex Matter, Jozef Stefan Institute, Jamova 39, 1000 Ljubljana, Slovenia*
[2] *Department of Physics, Loughborough University, Loughborough LE11 3TU, United Kingdom*
[3] *Department of Physics, Shanghai Jiao Tong University, Shanghai 200240, China*
[4] *National Laboratory for Ultrafast and Ultraintense Optical Science, INFM-CNR, Dipartimento di Fisica, Politecnico di Milano, 20133 Milano, Italy*

We determined electronic relaxation times via pump-probe optical spectroscopy using sub-15 fs pulses for the normal state of two different cuprate superconductors. We show that the primary relaxation process is the electron-phonon interaction and extract a measure of its strength, the second moment of the Eliashberg function $\lambda\langle\omega^2\rangle = 800 \pm 200$ meV^2 for $La_{1.85}Sr_{0.15}CuO_4$ and $\lambda\langle\omega^2\rangle = 400 \pm 100$ meV^2 for $YBa_2Cu_3O_{6.5}$. These values suggest a possible fundamental role of the electron-phonon interaction in the superconducting pairing mechanism.

PACS numbers: 78.47.J-, 74.72.-h, 42.65.Re, 71.38.-k

The electron-phonon interaction (EPI) is decisive for determining the functional properties of materials. It is the main scattering process governing electronic conductivity and is crucial for the formation of ordered electronic states such as charge-density waves and often the superconducting state. The determination of its strength - usually defined as the second moment $\lambda\langle\omega^2\rangle = 2\int_0^\infty \alpha^2F(\omega)\omega d\omega$ of the Eliashberg spectral function $\alpha^2F(\omega)$ [1] - is thus of fundamental importance. Standard methods for determining $\lambda\langle\omega^2\rangle$ experimentally from phonon linewidths in Raman or neutron scattering are often biased by selection rules and inhomogeneous broadening, and have given controversial results in the past. Since scattering from phonons is one of the main relaxation processes for electrons, $\lambda\langle\omega^2\rangle$ can be accurately extracted from the electron-phonon relaxation time τ_{e-ph}, provided that: (i) the experiment affords adequate time resolution to determine τ_{e-ph}, and (ii) an appropriate model connecting $\lambda\langle\omega^2\rangle$ and τ_{e-ph} is used. We will show in this paper that for materials with strong EPI, to satisfy both conditions, we need to go beyond current approaches. Here, by using optical spectroscopy with ultra-high time-resolution (< 20 fs instrument response) and a new, more appropriate model, we obtain $\lambda\langle\omega^2\rangle$ values for two high-critical temperature (T_c) cuprate superconductors, which allows us to assess the role of the EPI in the superconducting mechanism in these materials. Ultrahigh time-resolution is important to detect fast processes in strongly interacting systems, and to correctly identify the EPI relaxation in cases where the data contain the dynamics of several processes. Since for strong EPI τ_{e-ph} can be well below 100 fs, we need a better resolution than the usual 50-80 fs used so far [2–5]. Therefore we use state-of-the art ultrashort laser pulses from two synchronised non-collinear optical parametric amplifiers [6].

In femtosecond optical pump-probe spectroscopy the sample is excited with a short pump laser pulse, and the reflectivity is measured with a (weaker) probe pulse at a variable delay. The pump beam is periodically modulated and the photoinduced signal is expressed as a relative change of the reflected light intensity $\frac{\Delta R}{R} = \frac{R_{pump}-R_0}{R_0}$, where R_{pump} and R_0 are the reflected intensities with and without pump pulse, respectively. The temporal evolution of $\frac{\Delta R}{R}$, which - for small perturbations - is related to the temporal evolution of the dielectric constant $\Delta\epsilon/\epsilon$, is a direct signature of the energy relaxation processes in the sample. We used 15-fs pump pulses centred at 530 nm and broad band sub-10-fs probe pulses with a spectrum ranging from 500 to 700 nm (a detailed scheme is found in the supplementary information). This non-degenerate pump-probe configuration eliminates coherent interference artefacts. Single crystals of $YBa_2Cu_3O_{6.5}$ (YBCO, $T_c = 60$ K) and $La_{1.85}Sr_{0.15}CuO_4$ (LSCO, $T_c = 38$ K) were prepared as in ref. [7, 8]. To avoid any competing relaxation processes from emergent low temperature states (e.g. superconducting, pseudogap, antiferromagnetic, or stripe order), we performed all experiments at room temperature.

Until recently, a theoretical framework expressing τ_{e-ph} in terms of $\lambda\langle\omega^2\rangle$ has been provided by the so-called two-temperature model (TTM) [9, 10]. It is based on the assumption that the relaxation time due to electron-electron (e-e) collisions τ_{e-e} is much shorter than τ_{e-ph}. The e-e scattering is assumed to establish a thermal distribution of electrons with a temperature $T_e > T_l$ (T_l being the lattice temperature) on a time scale typically faster than the experimental time resolution. The relaxation time τ_{e-ph} of subsequent electron cooling via EPI is related to $\lambda\langle\omega^2\rangle$:

*To whom correspondence should be addressed: christoph.gadermaier@ijs.si

$$\lambda\langle\omega^2\rangle = \frac{\pi}{3}\frac{k_B T_e}{\hbar\tau_{e-ph}} \quad (1)$$

This expression has been used in the analysis of transient optical experiments [2–4], and recently also time-resolved angle-resolved photoemission spectroscopy (ARPES) [5]. For the typical laser fluences used in these experiments T_e is in the range 400-800 K . This gives an estimate for $\tau_{e-e} = 350$ fs $\div$ 1.4 ps, depending on the fluence (see supplementary information). From Eq. (1), τ_{e-ph} is expected to be proportional to T_e and thus vary significantly over the range of fluences used in the experiment.

Outside the TTM regime, the relaxation behavior can be described via the kinetic Boltzmann equation using e-e and e-ph collision integrals, where the electrons and phonons are both out of equilibrium. This has been done both numerically [11] and recently also analytically [12, 13]. The calculated electron distribution based on the analytical solution of this non-equilibrium model (NEM) [13] departs from the equilibrium Fermi-function particularly for high energies. (A comparison with published time-resolved ARPES data is shown in the supplement.) The analytical treatment yields a relation:

$$\lambda\langle\omega^2\rangle = \frac{2\pi}{3}\frac{k_B T_l}{\hbar\tau_{e-ph}}. \quad (2)$$

which is applicable also when $\tau_{e-e} > \tau_{e-ph}$. Besides the factor 2, a notable difference compared to the TTM formula (Eq. (1)) is that τ_{e-ph} is predicted to be linearly dependent on T_l (not T_e). Since the heat capacity of the lattice is much higher than that of electrons, in our experiments T_l is close to room temperature for all fluences, so we expect that τ_{e-ph} should be independent of fluence. This provides a critical test of the model's applicability.

The experimental data for LSCO (Figs 1a+b)) and YBCO (Figure 1c)) show a fast initial decay followed by a slower dynamics, all of which are independent of laser fluence. We fit the transient response of both cases (see Figs 1b+c) with two exponential decays with time constants τ_a and τ_b respectively, and a long-lived plateau, using the pump-probe cross-correlation as the generation term. For each sample, the same τ_a and τ_b are obtained at different probe wavelengths. YBCO also contains an oscillatory response due to impulsively excited coherent phonons. This coherent phonon contribution can be removed almost entirely by fitting the oscillatory response of the known Raman-active modes and subtracting it from the data (see Fig. 1c)). The fact that in YBCO at 520 nm the two signal components have opposite sign nicely confirms that we are actually observing two processes and not at a non-exponential process which could accidentally be fitted with two exponentials. The fit yields $\tau_a = 45 \pm 8$ fs and $\tau_b = 600 \pm 100$ fs for LSCO and $\tau_a = 100 \pm 20$ fs and $\tau_b = 450 \pm 100$ fs for YBCO respectively. This behavior is systematically observed over the whole spectral range of our probe pulse between 500 and 700 nm (see supplementary information).

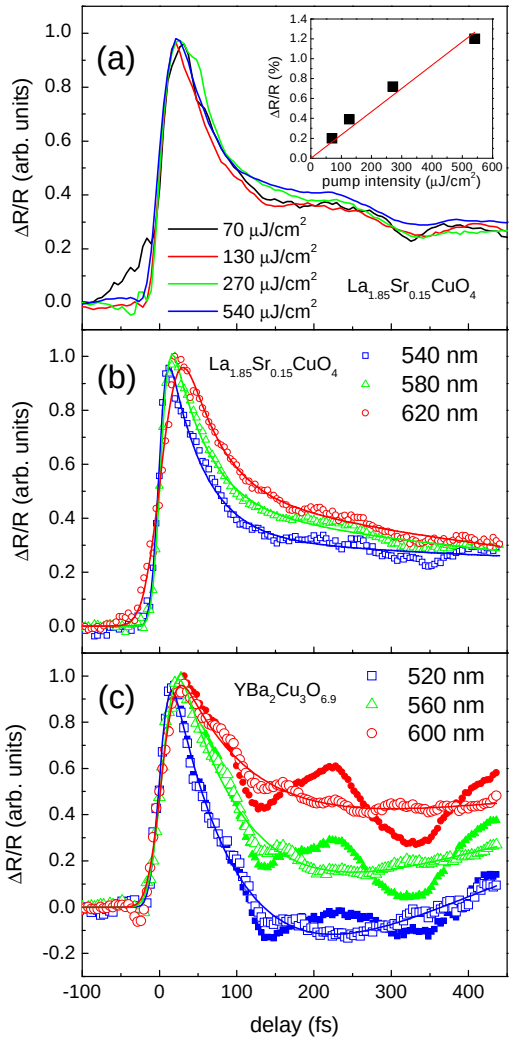

Figure 1: a) Normalised photoinduced reflectivity change in $La_{1.85}Sr_{0.15}CuO_4$ at 590 nm for different pump intensities. The inset shows the signal magnitude as a function of pump intensity. b) $\Delta R/R$ of $La_{1.85}Sr_{0.15}CuO_4$ at different probe wavelengths (symbols) and double-exponential fits (lines). c) $\Delta R/R$ of $YBa_2Cu_3O_{6.5}$ at different probe wavelengths and double-exponential fits. Small full symbols show the original data, large open symbols show the data after subtraction of three oscillating modes at 115, 145, and 169 cm^{-1}. These oscillations arise from a modulation of the reflectivity by phonons coherently excited in the sample by the pump pulse, whose duration is much shorter than the oscillation period [15, 16]. The three modes are known from Raman spectroscopy [17, 18].

Since the observed dynamics is fluence independent (see Figure 1a), neither of the two fast relaxation processes can be attributed to $e-e$ scattering. Following previous studies [4, 5], we assign τ_a to relaxation via the

EPI mechanism. The origin of the longer relaxation time τ_b has been discussed in detail previously [4, 5, 8, 14] and is of no further interest here.

The choice of model (TTM or NEM) for determining $\lambda\langle\omega^2\rangle$ from τ_{e-ph} is based on the relatively stringent requirement regarding the fluence dependence of τ_{e-ph}. A fluence-dependent τ_{e-ph} is clearly not observed here, and to the best of our knowledge has never been observed in cuprates. We thus conclude that the TTM is not applicable, while the data are consistent with the NEM solution without the assumption that $\tau_{e-e} << \tau_{e-ph}$. Calculating the EPI strength, Eq. (2) yields $\lambda\langle\omega^2\rangle = 800 \pm 200$ meV^2 for LSCO and $\lambda\langle\omega^2\rangle = 400 \pm 100$ meV^2 for YBCO. As additional confirmation regarding the choice of model, we note that a dependence of τ_{e-ph} on the sample temperature, as predicted by the NEM *has* actually been observed in cuprates [19] and superconducting iron pnictides [20] above the pseudogap temperature, where it is expected to apply. No such dependence is predicted by the TTM.

To assess the consequences of using the NEM rather than the traditional TTM, in the supplementary information we compare $\lambda\langle\omega^2\rangle$ values obtained with the two models both for our data and for several metals from the literature. The TTM assumption $\tau_{e-e} << \tau_{e-ph}$ is generally not valid. The discrepancy in $\lambda\langle\omega^2\rangle$ calculated with the two models can be up to a factor of 2. If different fluences are used, as in our data, the variation of T_e introduces an additional uncertainty if we use the TTM estimate.

To obtain an estimate of λ from the data, we express the second moment of the Eliashberg function as the product of a dimensionless electron-phonon coupling constant λ and the square of a characteristic phonon frequency ω_0: $\lambda\langle\omega^2\rangle = \lambda\omega_0^2$. The estimate of ω_0 and consequently λ requires a detailed knowledge of the Eliashberg spectral function. This can be extracted from other experiments such as optical absorption [21, 22], neutron scattering [23–25], ARPES [26, 27], and tunnelling [28–33]. Based on these references the best estimate of ω_0 is about 40 meV, which gives $\lambda \gtrsim 0.5$ for LSCO and $\lambda \gtrsim 0.25$ for YBCO. Remarkably, these values agree very well with ab initio calculations that predict 0.27 for YBCO [34] and 0.4 for LSCO [35, 36].

To assess the possible contribution of EPI to the superconductive pairing mechanism in the cuprates, we briefly discuss the observations in terms of existing theories based on phonon mediated pairing – most notably BCS theory and polaronic pairing [37–40]. BCS theory predicts that $k_B T_c = \hbar\omega_0 \exp[-(1+\lambda)/\lambda]$ (if any repulsive Coulomb pseudopotential is neglected). At maximum (λ=2, ω_0=$\sqrt{\lambda\langle\omega^2\rangle/2}$, see supplementary information) the BCS critical temperature can be $T_c^{max} = 52$ K for LSCO and only $T_c^{max} = 37$ K for YBCO. Remarkably - contrary to the experiment - it predicts a *higher* T_c for LSCO than for YBCO.

Polaronic pairing within the band picture, on the other hand, yields a maximum $T_c(\lambda)$ that is significantly higher than for BCS and is obtained at a lower λ value. Polaronic band-narrowing due to phonon "dressing" of carriers strongly enhances the density of states in a narrow polaron band and consequently also the critical temperature of polaronic superconductors [37]. With further increase of the EPI strength carriers form real-space (bipolaronic) pairs and the critical temperature, which is now the Bose-Einstein condensation temperature, drops since the effective mass of these composed bosons increases [38]. The highest $T_c(\lambda)$ exceeding the BCS value by several times is hence found in the intermediate crossover region of the EPI strength from the weak-coupling BCS to the strong-coupling polaronic superconductivity. Strong e-e correlations increase the effective mass of carriers (or decrease the bare band-width), and heavier carriers form lattice polarons at a smaller value of λ [41, 42] ($\lambda_c \approx 0.9$ for uncorrelated 2D polarons [43], while $\lambda_c \lesssim 0.4$ in the Holstein t-J model [42]). The observed EPI strengths are therefore consistent with polaronic pairing in the presence of strong electron correlations, whereby YBCO lies in the crossover region close to the maximum T_c, while LSCO would appear to be on the strong-coupling side of this region ($\lambda > \lambda_c$). Alternatively, within local bipolaron pairing models [39], the limits of T_c are set by (dynamic or static) phase coherence percolation [44], where the interplay of the EPI and the Coulomb repulsion between doped carriers V_c determine the pair density and detailed real-space texture [40]. These models give a charge-ordered regime when Coulomb repulsion dominates ($\lambda/N_0 \ll V_c$, with N_0 being the density of states at the Fermi energy) and a fully phase separated state when EPI is dominant ($\lambda/N_0 \gg V_c$). In the crossover region between these two regimes, a textured state favoring pair (bipolaron) formation exists, leading to superconductivity with a distinct maximum T_c.

Our results reinforce the other compelling experimental evidence for a strong role for the EPI in cuprates obtained from isotope effects [33], high resolution ARPES [26, 27], optical [21, 22], neutron-scattering [23–25], and tunnelling [31, 32, 45] spectroscopies. However, our data on two materials can only demonstrate the realistic feasibility of the polaronic pairing mechanism, and cannot rule out any non-phononic contribution to the pairing. Indeed part of the glue function has been identified with an energy well above the upper limit of the phonon frequencies in the cuprates (100 meV) [46]. While this could be a signature of multi-phonon dressing of carriers, spin and/or electron density fluctuations might be alternative mechanisms of the high-energy glue. By using the appropriate theory and adequate time resolution, as we have shown, one can now collect accurate data for further cuprate high-T_c materials to decide whether the agreement with the polaronic mechanism is coincidental or systematic. Similar work will be of fundamental significance for other effects where EPI is important, such as high T_c superconductivity in non-cuprate materials (notably iron-pnictides [20]), colossal magnetoresistance, the formation of orbitally-ordered states and charge density

waves.

Acknowledgments

This work was supported by the Slovenian Research Agency (ARRS) (grants J1-2305, 430-66/2007-17 and BI-CN/07-09-003), EPSRC (UK) and the Royal Society (grants EP/D035589/1 and JP090316), MOST of China (Project 2006CB601003), and by the European Commission [grants EIF-040958A, ERG-230975, and the European Community Access to Research Infrastructure Action, Contract RII3-CT-2003-506350 (Centre for Ultrafast Science and Biomedical Optics, LASERLAB-EUROPE)]. We thank S. Sugai for the $La_{1.85}Sr_{0.15}CuO_4$ sample and D. Polli and L. Stojchevska for fruitful discussions.

[1] G.M. Eliashberg, *Zh. Eksp. Teor. Fiz.* **38**, 966 (1960); **39**, 1437 (1960) [*Sov. Phys. JETP* **11**, 696; **12**, 1000 (1960)].
[2] Brorson, S.D. et al. *Phys. Rev. Lett.* **64**, 2172 (1990).
[3] S. V. Chekalin *et al.*, *Phys. Rev. Lett.* **67**, 3860 (1991).
[4] J.-X. Zhu *et al.*, arXiv:0806.2664. (2008).
[5] L. Perfetti *et al.*, *Phys. Rev. Lett.* **99**, 197001 (2007).
[6] C. Manzoni, D. Polli, and G. Cerullo, *Rev. Sci. Instrum.* **77**, 023103 (2006).
[7] H. Gao *et al.*, *Phys. Rev. B* **74** 020505(R) (2006).
[8] P. Kusar *et al.*, *Phys. Rev. Lett.* **101**, 227001 (2008).
[9] M. I. Kaganov, I. M. Lifshits, and L. B. Tanatarov, *Zh. Eksp. Teor. Fiz.* **31**, 232, (1956) [*Sov.Phys. JETP* **4**, 173 (1957)].
[10] P. B. Allen, *Phys. Rev. Lett.* **59**, 1460 (1987).
[11] R. H. M. Groeneveld, R. Sprik, and A. Lagendijk, *Phys. Rev. B* **51**, 11433 (1995).
[12] V. E. Gusev and O. B. Wright, *Phys. Rev. B* **57**, 2878 (1998).
[13] V. V. Kabanov and A. S. Alexandrov, *Phys. Rev. B* **78** 174514 (2008).
[14] V. V. Kabanov, J. Demsar, B. Podobnik, and D. Mihailovic, *Phys. Rev. B* **59**, 1497 (1999).
[15] J. M. Chwalek *et al.*, *Appl. Phys. Lett.*. **58**, 980 (1991).
[16] A. Kutt, W. Albrecht, and H. Kurz, *IEEE J. Quantum Electron.* **QE-28**, 2434 (1992).
[17] E. T. Heyen *et al.*, *Phys. Rev. Lett.* **65**, 3048 (1990).
[18] M. N. Iliev *et al.*, *Phys. Rev. B* **77**, 174302 (2008).
[19] Y. H. Liu *et al.*, *Phys. Rev. Lett.* **101**, 137003 (2008).
[20] T. Mertelj *et al.*, arXiv:1001.1047. (2010).
[21] D. Mihailovic, C. M. Foster, K. Voss, and A. J. Heeger, *Phys. Rev. B* **42**, 7989 (1990).
[22] R. Zamboni, G. Ruani, A. J. Pal, and C. Taliani, *Solid St. Commun.* **70**, 813 (1989).
[23] M. Arai *et al.*, *Phys. Rev. Lett.* **69**, 359 (1992).
[24] T. Egami, *J. Low Temp. Phys.* **105**, 791 (1996).
[25] D. Reznik *et al.*, *Nature* **440**, 1170 (2006).
[26] A. Lanzara *et al.*, *Nature* **412**, 510 (2001).
[27] W. Meevasana *et al.*, *Phys. Rev. Lett.* **96**, 157003 (2006).
[28] S. I. Vedeneev *et al.*, *Phys. Rev. B* **49**, 9823 (1994).
[29] J. F. Zasadzinski, L. Coffey, P. Romano, Z. Yusof, *Phys. Rev. B* **68**, 180504(R) (2003).
[30] X. J. Zhou *et al.*, *Phys. Rev. Lett.* **95**, 117001 (2005).
[31] J. Lee *et al.*, *Nature* **442**, 546 (2006).
[32] H. Shim, P. Chaudhari, G. Logvenov, and I. Bozovic, *Phys. Rev. Lett* **101**, 247004 (2008).
[33] G. M. Zhao, in *Polarons in Advanced Materials* (ed. A. S. Alexandrov, Springer, New York, 2007), vol. **103** of *Springer Series in Material Sciences*, p. 569 ; A. Bussmann-Holder and H. Keller, ibid, p. 600.
[34] K.-P Bohnen, R. Heid, and M. Krauss, *Europhys. Lett* **64**, 104 (2003).
[35] F. Giustino, M. L. Cohen, and S. G. Louie, *Nature* **452**, 975 (2008).
[36] D. Reznik, G. Sangiovanni, O. Gunarsson, and T. P. Devereaux, *Nature* **455**, E6 (2008).
[37] A. S. Alexandrov, *Zh. Fiz. Khim.* **57** 273 (1983) [*Russ. J. Phys. Chem.* **57**, 167 (1983)].
[38] A. S. Alexandrov, *Phys. Rev. B* **38**, 925 (1988).
[39] K. A. Müller, *J. Phys.: Condens. Matter* **19**, 251002 (2007).
[40] T. Mertelj, V. V. Kabanov, and D. Mihailovic, *Phys. Rev.Lett.* **94**, 147003 (2005).
[41] H. Fehske, H. Roder, G. Wellein, and A. Mistriotis, *Phys. Rev. B* **51**, 16582 (1995).
[42] A. S. Mishchenko and N. Nagaosa, in *Polarons in Advanced Materials* (ed. A. S. Alexandrov, Springer, New York, 2007), vol. **103** of *Springer Series in Material Sciences*, p. 533.
[43] V. V. Kabanov and O. Y. Mashtakov, *Phys. Rev. B* **47**, 6060 (1993).
[44] D.Mihailovic, V.V.Kabanov and K.A.Müller. Europhys Lett. **57**, 254 (2002).
[45] G. M. Zhao, *Phys. Rev. Lett.* **103**, 236403 (2009).
[46] E. van Heumen *et al.*, *Phys. Rev. B* **79**, 184512 (2009).